J. Min. Metall. Sect. B-Metall. 58 (1) (2022) 29 - 41

Journal of Mining and Metallurgy, Section B: Metallurgy

EFFECT OF TITANIUM CONTENT ON THE MICROSTRUCTURE AND WEAR BEHAVIOR OF $Fe_{(13-x)}Ti_xB_7$ (x=0-5) HARDFACING ALLOY

B. Kılınç [a,*], E. Kocaman [b], Ş. Şen [c], U. Şen [c]

[a] Sakarya University of Applied Sciences, Machine and Metal Program, Vocational School of Arifiye, Arifiy, Sakarya, Turkey

[b] Zonguldak Bülent Ecevit University, Faculty of Engineering, Department of Metallurgical and Materials Engineering, İncivez, Zonguldak, Turkey

[c] Sakarya University, Faculty of Engineering, Department of Metallurgical and Materials Engineering, Esentepe Campus, Sakarya, Turkey

(Received 30 April 2021; Accepted 06 August 2021)

Abstract

In this study, the effects of titanium addition on microstructure, hardness, and wear rate of $Fe_{(13-x)}Ti_xB_7$ (x = 0, 1, 2, 3 and 5) based hard surface alloy layers formed by gas tungsten arc (GTA) welding method were investigated. As a result of the microstructure studies and phase analysis, it was determined that the structures of the coating layers consisted of α-Fe, αFe+Fe_2B eutectic, α-Fe+Fe_2Ti eutectic and hard TiB_2 phases. In the hard surface alloy layer, as the amount of titanium was increased, the TiB_2 phase density formed in the system increased and it was observed that rod-like and long sharp-edged phases formed from the equiaxed structure. As a result of wear tests performed at different loads, it was determined that the addition of titanium reduces the wear rates in the coating layers. In addition, scanning electron microscopy (SEM) images of the worn surfaces showed that the wear mechanisms were adhesive and oxidative.

Keywords: *Hardfacing; Surface alloying; Fe-Ti-B alloy; Boride; Hardness; Wear*

1. Introduction

Hard surface alloying is a form of surfacing commonly used to improve the surface properties of agricultural tools, mining components, soil preparation equipment, and other machine components [1–3]. This process is applied to increase the hardness and wear resistance of the substrate material without any significant loss in ductility and toughness. With this method, an alloy is homogeneously deposited on the surface of a soft material (generally low and medium carbon steels) by various welding techniques [2].

Among these techniques, gas tungsten arc (GTA) welding has an important place with advantages such as high deposition rate, high maneuverability, large-scale availability, low cost and compatibility with a wide variety of materials [4–7]. In this regard, the desired composition powder and the surface of substrate material are melted simultaneously by the GTA welding process and a layer of alloy that is metallurgically bonded to the base material is formed by solidification [8, 9].

Titanium borides have many advantages such as high melting point, hardness, wear resistance and electrical conductivity. Titanium-boron binary phase diagram contains compounds such as TiB, Ti_3B_4, and TiB_2 [10]. TiB_2 has found a wide use in ceramic reinforced composites synthesized in-situ with iron and steel matrix due to its high melting temperature, low density, good thermal and chemical stability, and high hardness [11–13]. The potential application areas of titanium borides are quite wide, including impact resistant armors, cutting tools, wear resistant parts, grain refiners and all kinds of high temperature structural materials. In addition, its high electrical conductivity enables titanium borides to be used in electrical discharge process. For this reason, more experimental and theoretical research has been started on these borides in recent years [10]. Wang et al. [11] produced steel matrix composite coatings reinforced with in-situ TiC-TiB_2 particles using argon arc welding technique and investigated the microstructure, micro hardness, and wear properties of the produced coatings. As a result of the investigations, they determined that the main phases in the coating are TiC, TiB_2, and α-Fe and that a perfect metallurgical bond was formed between the composite coating and the substrate. They have also observed that the coating is uniform, continuous, and

*Corresponding author: bkilinc@subu.edu.tr

https://doi.org/10.2298/JMMB210430047K

almost flawless, with the reinforcing particles dispersed in the produced coating in a distributed manner. They determined that with the increase of the dispersed TiC+TiB_2 content in the coating, the micro hardness and corrosion resistance of the coating improved under normal atmospheric conditions and room temperature. Yılmaz et al. [14] manufactured TiB_2-reinforced Fe-based coatings synthesized in-situ by GTA welding on AISI 4340 steel substrate and experimentally investigated the effects of process parameters on the coating. In the investigations, primary dendrites and complex TiB_2, Fe_2B borides in ferrite (α) phase were detected on the coating surface, and it was observed that the coated surface or interface microstructures were formed by the distribution of boron and titanium concentrations. Darabara et al. [15] obtained Fe_2B-TiB_2 reinforced metal matrix composite (MMC) hard surface layer on a flat steel surface using plasma transfer arc (PTA) welding technique. For this process, five different powder compositions were obtained by increasing the boron content and the hard surface alloy layers were produced from these powders. The microstructures of the hard surface alloy layers produced were examined, phase analyzes were made, and their hardness was measured. As a result, it has been determined that increasing the boron content causes an increase in the micro hardness of hard iron boride particles due to the presence of Fe_2B.

Although there are many studies in the literature on hardening the surfaces of steels and alloys containing boron, studies on Fe-Ti-B hard surface alloy processes are limited. In this study, Fe-Ti-B based coatings were produced by using cost-effective ferro alloys by GTA welding method on low carbon steel. The aim of this study was to investigate the effects of titanium in the produced alloy system on the microstructure and mechanical properties of the coating layer.

2. Experimental procedure

In this study, SAE 1320 steel cut to size 30 mm x 70 mm x 5 mm was used as the substrate material for the hard surface alloying process. The chemical composition of SAE 1320 steel selected as a substrate material is given in Table 1. The surfaces of these plates were cleaned from oil, rust and dirt layer for hard surface alloying process.

In the experimental studies performed, ferrous boron, ferrous niobium alloys, and ASC100.29 coded pure iron powder were used. Compositions of ferrous alloys and pure iron used to form boride based hard surface alloys are given in Table 2.

Table 1. *Chemical composition of the substrate (wt.%)*

	C	Cr	Mn	Si	P	S	Ni	Mo	Fe
Comp.	0.183	0.0208	1.37	0.204	0.0177	0.0018	0.062	0.0056	98

Table 2. *Composition of used powders (wt.%)*

Powders	Fe	B	Ti	C	Al
Ferro-boron	82	18	-	-	-
Ferro-titanium	25.22	-	70.95	0.126	3.69
Pure iron	99.9	-	-	-	-

Ferrous alloys which were taken as a rock form was subjected to crushing, grinding, and sieving processes to be less than 75 µm. Pure iron powder was only sieved. The prepared powders were determined in the composition ratios given in Table 3 to form Fe-B, Fe-Ti-B based hard surface alloys and mixing was carried out.

Table 3. *Combination rates of powders prepared for $Fe_{(13-x)}Ti_xB_7$ (x=0, 1, 2, 3 and 5) based surface alloys (at.%)*

Metal Alloy	Compositions	Fe	Ti	B
Fe-B	$Fe_{13}B_7$	65	-	35
Fe-Ti-B	$Fe_{12}TiB_7$	60	5	35
	$Fe_{11}Ti_2B_7$	55	10	35
	$Fe_{10}Ti_3B_7$	50	15	35
	$Fe_9Ti_5B_7$	40	25	35

Fe-Ti-B ternary phase diagram [16] was used to determine the composition ratios. Prepared powders were subjected to milling and mixing for 2 hours at 200 rpm in a ball mill to ensure a homogeneous composition distribution. Powder / ball ratio was selected as 1/3 and steel balls with 7 mm diameter were used in the mixing process. Before mixing, the containers and balls were thoroughly cleaned with pure alcohol. Powder mixtures were placed on the prepared substrates with a thickness of about 2-3 mm and pressed under pressure of 100 MPa with the help of hydraulic press before welding. Thus, the negativity caused by gas pressure during GTA welding process was eliminated.

Fe-Ti-B based mixture powders formed by pressing on steel substrates were melted by GTA welding method and alloy was formed on the surface. Hard surface alloy coating processes were carried out with Magmaweld ID 220T AC / DC Pulse TIG inverter welding machine. After the process, the samples were cooled in the open atmosphere and subjected to sand blasting to remove the oxide layers and burrs formed during welding. The welding parameters applied during the process are shown in Table 4.

Table 4. *Experimental Parameters of GTA Surface alloying. Heat input Q= η.U.I/(V.1000) (kj/cm); U: voltage (V), I: current (A), V: travel speed (cm/sec), η = efficiency coefficient (η = 0.65 for the GTA method) [17].*

Parameter	Value
Electrode	Type WT-2 pct ThO_2
Electrode Diameter	2.4 mm
Angle	70 degrees
Voltage	20 V
Current	180 A
Heat input	20.2 kJ/cm
Protective gas	Type Ar (%99.9 Ar)
Flow	12 L/min
Welding speed	0.116 cm/sec

The samples were prepared according to standard metallographic procedure by grinding, polishing and etching with (3%) Nital reagent, respectively. Microstructural characterization of the samples was carried out by using a Nikon Epiphot 200 optical microscope (OM) and JEOL-JSM-6060 scanning electron microscopy (SEM/EDS). An X-ray diffraction (XRD) was detected with Rigaku XRD/D/MAX/2200/PC model X-ray diffractometer using Cu-Kα radiation. The macro-hardnesses taken from the outer surfaces of the alloy layers were measured with a Rockwell (C scale) Bulut brand hardness tester by measuring from in three separate regions under 150 kg load. The hardness of the phases formed in the alloyed layer, transition zone and matrix were measured under 0.1 N load by using Future Tech FM 700 micro-hardness tester.

The surfaces of steels alloyed by the GTA welding method were metallographically prepared before the wear test. For this purpose, coarse polishing process was applied to the alloyed surfaces with abrasive papers of 60, 120, 240, 400, 600, 800, and 1000 grit. The wear tests of the hard surface coated samples were carried out on the tribometer device in accordance with the ASTM G-99 standard. Experiments were carried out using Ball-On Disk method, using a 10mm diameter alumina (Al_2O_3) balls with a hardness value of 2720 HV0.05 [18]; It was carried out under 2.5N, 5N, and 10N loads at 200 m distance and 0.1 m/s speed, 65±5 relevant humidity, and 21±3 ºC temperature in an open atmosphere. The volume from the wear track was measured using the cross-sectional area of the wear track (A), which was determined using 3D optical microscopes (Huvitz). In the measurements, the standard deviation on the worn track was typically less than 10% of its average value. The wear volume, V_d, was calculated using Eq. (1) [19]:

$$V_d = 2\pi rA \quad (1)$$

where r is the radius of the wear track, and A is the worn track cross-sectional area that was calculated from the profile of the wear track. Finally, the wear track formed on the disks was examined using optical microscopy, scanning electron microscopy and energy dispersive X-ray spectroscopy (EDS).

3. Results and discussion

3.1. Microstructural and Phase analysis

Optical microstructure of $Fe_8Ti_5B_7$ hard surface alloy produced by TIG welding method is given in Figure 1. As a result of the microstructure studies, it was determined that the thickness of the hard coated layer was approximately 2-3 mm and that it showed good bonding with the substrate. It was determined that this rather thick coating layer has a smooth surface topography without porosity. In the examined microstructures, a structure consisting of three different layers such as hard surface layer, interface, and substrate can be clearly distinguished.

SEM microstructure images of the Fe-B based alloy ($Fe_{13}B_7$) formed on the steel surface are given in Figure 2 (a). When the microstructures were examined, it was found that eutectic (α-Fe+Fe_2B) phases were observed together with the hypereutectic primary Fe_2B massive phase.

In the study of Eroğlu [20], Fe-B based filler alloys were selected as hypoeutectic and hypereutectic alloys and the solidification structures were examined. He stated that in the solidification of hypereutectic structures, firstly FeB (few) and the primary Fe_2B phase grew by nucleation in the liquid phase and the structure transformed into a eutectic (γFe + Fe_2B) structure with the primary Fe_2B massive phase at 1174 ºC. He explained that with the decreasing temperature, the γ-Fe phase in the system transformed into martensite phase and the eutectic (martensite + Fe_2B) phases / structures were formed with hypereutectic the primary Fe_2B massive phase and FeB (few). When the Fe-B phase diagram is examined [21], it is seen that the

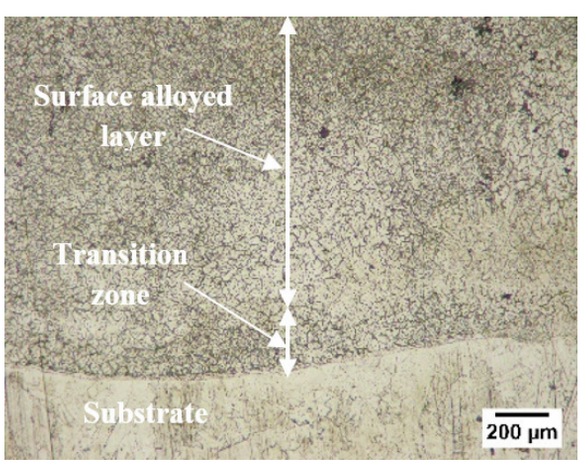

Figure 1. *Cross-section of $Fe_8Ti_5B_7$ hard surface alloy*

solidification for hypereutectic compounds will be similar to Eroğlu's explanations. However, as a result of the analysis, FeB and martensite phases were not found in the coating layer. It is an expected situation since the formation of these phases will take place under out of equilibrium conditions. In addition, the x-ray diffraction pattern given in Figure 4 shows that the $Fe_{13}B_7$ based alloy consists of α-Fe and Fe_2B phases. As a result, it is possible to say that the Fe-B coating layer formed on the steel surface consists of the primary Fe_2B block phase and the eutectic (α-Fe+Fe_2B) phase.

Figure 2 shows the locations of the produced hard surface alloys in the Fe-Ti-B equilibrium diagram at 1000 °C. It is understood that hard surface alloys are on the iron-rich side of the Fe-Ti-B system. According to the isothermal diagram, possible phases that may occur in alloys that solidify in this range are α-Fe, γ-Fe, Fe_2B, TiB_2 and Fe_2Ti.

In the SEM microstructure of $Fe_{(13-x)}Ti_XB_7$ (x= 0, 1, 2, 3, and 5) alloys (Figure 3 (b-e)), the presence of primary α-Fe phases and the eutectic structure of the α-Fe and Fe_2B phases are observed. In addition, in the microstructure studies (Figure 3 (b)), it was determined that when 5% Ti was added to the alloy at atomic rate, homogeneously dispersed (especially at grain boundaries) black colored TiB_2 phases of approximately 2-4 micron dimensions were formed in the coating layer.

SEM image EDS analysis and elemental distribution maps (MAP) of the $Fe_{(13-x)}Ti_xB_7$ sample given in Figure 4 (a) show that the black colored block phases contain titanium and boron elements, and the gray colored phases contain iron. For this reason, it is thought that the block gray colored phases are α-Fe and the black dispersed phases are TiB_2. As a result of EDS and MAP analysis (Figure 4 (b-h)), the eutectic structure located between α-Fe phases is thought to be composed of α-Fe and Fe_2B phases. X-ray diffraction analysis (Figure 5) shows that the $Fe_{(13-x)}Ti_XB_7$ system contains Fe_2Ti phases as well as α-Fe, Fe_2B and TiB_2 phases. As it can be understood from here, it was determined that the system consists of TiB_2 phases with α-Fe+Fe_2B and α-Fe+Fe_2Ti structure, which have eutectic morphology between the primary α-Fe phases.

In the study of Zdziobek et al. [22], it was shown that TiB_2 phases were formed primarily during the solidification of Fe-Ti-B alloy at an atomic rate of 5% Ti and 35% B. Then, it was shown that the δ-Fe phase solidified around TiB_2 phases, the δ-Fe transformed into γ-Fe depending on the temperature decrease, and γ-Fe+Fe_2B eutectic structure formed from the remaining liquid as the temperature decreased.

In the microstructure studies of $Fe_{(13-x)}Ti_XB_7$ (x= 0, 1, 2, 3 and 5) based alloys formed on the steel surface, it is seen that the TiB_2 phase formed in the system increases as the amount of Ti is increased. This is expected when the Fe-Ti-B ternary equilibrium

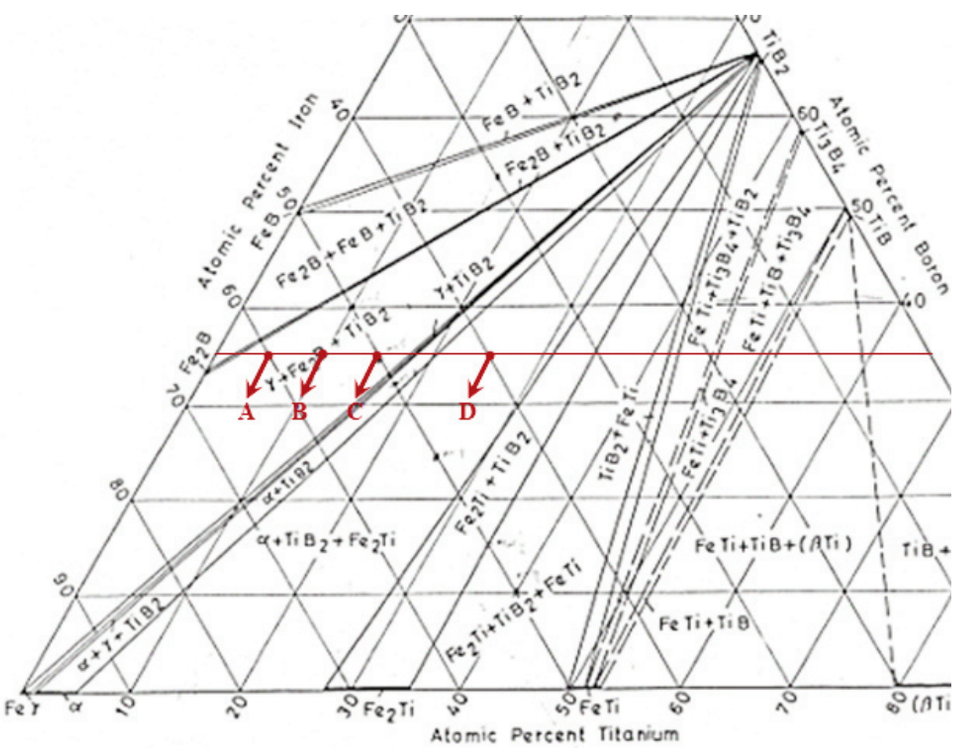

Figure 2. *Hard surface coating compositions in the isothermal section of Fe-Ti-B at 1000 °C [16] (A) $Fe_{12}TiB_7$ (B) $Fe_{11}Ti_2B_7$ (C) $Fe_{10}Ti_3B_7$ (D) $Fe_8Ti_5B_7$*

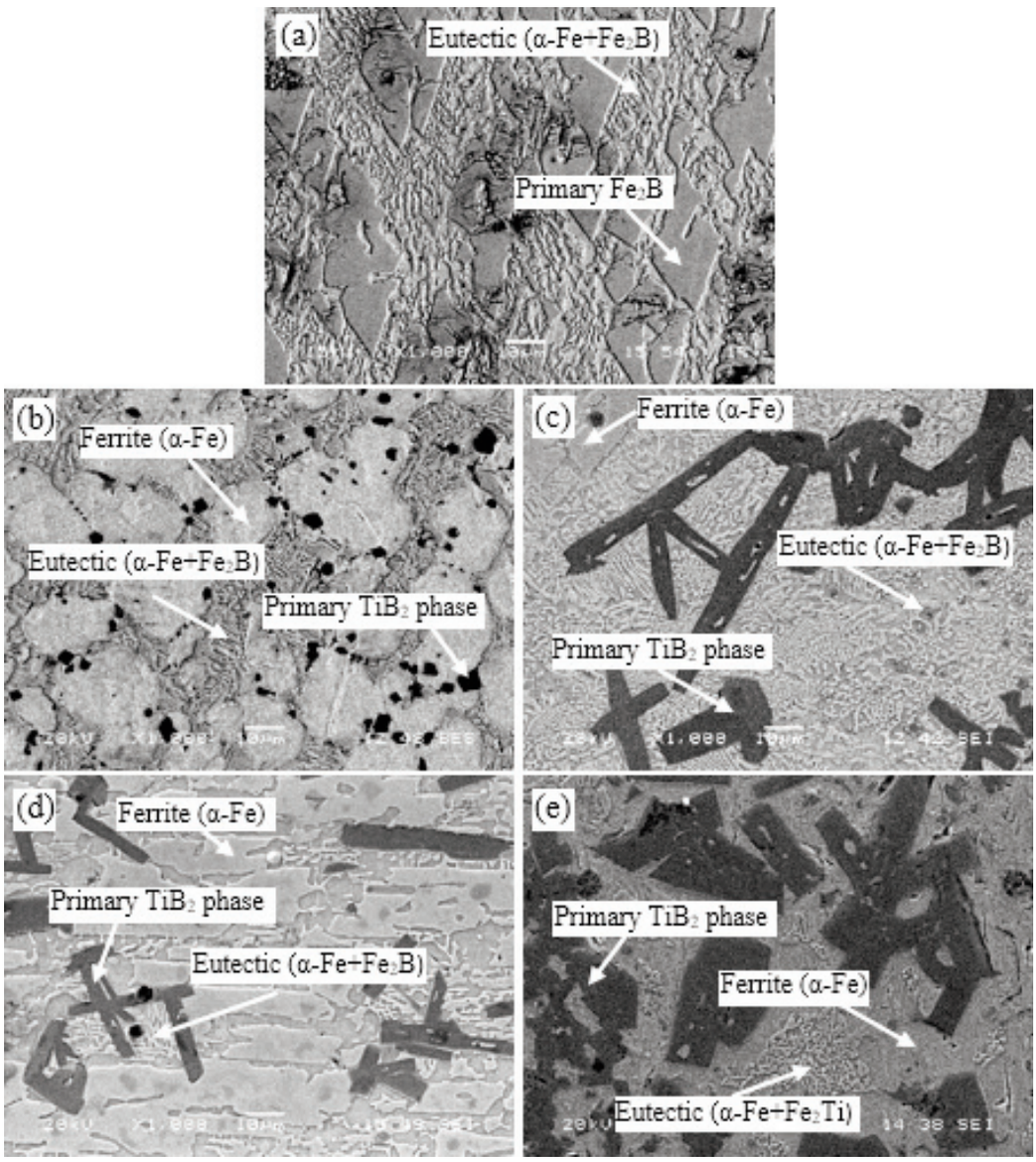

Figure 3. *SEM microstructure images of hard surface coating layers (a) $Fe_{13}B_7$ (b) $Fe_{12}TiB_7$ (c) $Fe_{11}Ti_2B_7$ (d) $Fe_{10}Ti_3B_7$ (e) $Fe_8Ti_3B_7$*

diagram is examined [16]. However, in microstructural studies, it is seen that the homogeneously distributed equiaxed TiB_2 structure appears as rod-like and long sharp-edged phase formations besides the equiaxed structure with the Ti content increasing to 10%. It is seen that the primary α-Fe phase is not observed here, whereas the TiB_2 phase is completely surrounded by the eutectic structure (α-Fe+Fe_2B). Again, in the microstructure, the partial existence of Fe_2B block phases apart from the eutectic structure was also detected.

As can be seen from the Fe-Ti-B equilibrium diagram, increasing the amount of Ti causes a decrease in Fe_2B and an increase in TiB_2 phase. In addition, depending on the temperature, α-Fe or γ-Fe solid solution is located next to these phases. When Ti amount increases to 15% atomically, the amount of TiB_2 phase formed increases and the eutectic structure (α-Fe+Fe_2B) decreases while primary α-Fe increases. However, when Ti content increases from 15% to 25%, TiB_2 increases a little more, and Fe_2Ti phase occurs instead of Fe_2B. In addition, the primary α-Fe phase is also included in the system. Again, when the structure is examined, the eutectic structure (α-Fe+Fe_2Ti) shows itself as small islets in the microstructure. Since the system includes melting and rapid solidification processes, it includes α-Fe, TiB_2, and Fe_2Ti phases as well as α-Fe+Fe_2B eutectic islets

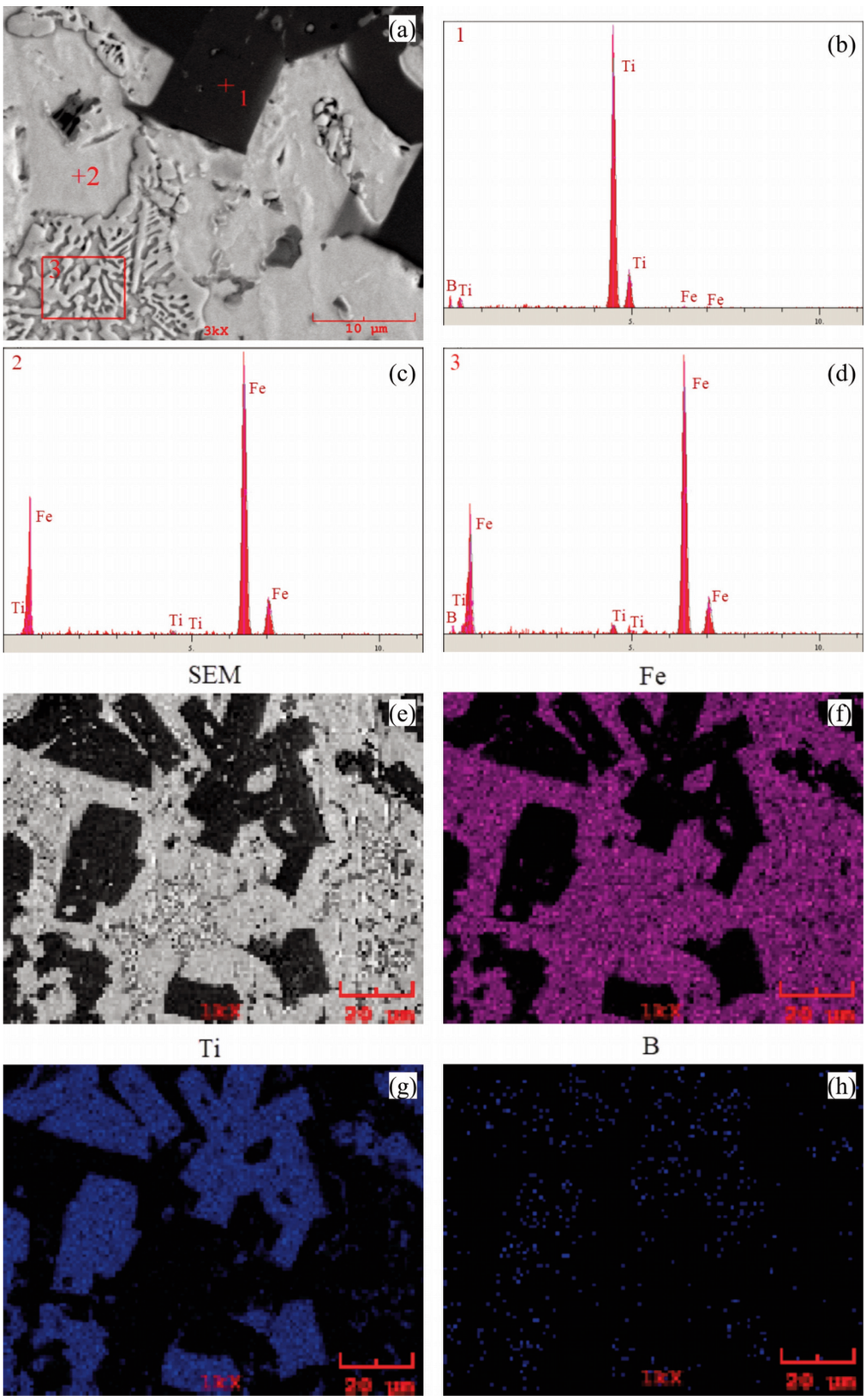

Figure 4. *(a) SEM image (b-d) EDS analysis and (e-h) elemental distribution maps of the hard surface alloy layer of $Fe_8Ti_3B_7$ sample*

that should be in the equilibrium diagram.

Generally, as the Ti ratio increases, the TiB_2 phase increases while the Fe_2B phase ratio decreases, and if titanium reaches very high rates, the Fe_2Ti phase emerges in the eutectic structure. This situation is compatible with the Fe-Ti-B equilibrium diagram and is similar to the study of Zdziobek et al. [22].

3.2. Hardness Measurements

Figure 6 shows the HRC hardness values measured from the surfaces of the hard surface alloyed samples. As a result of the hardness measurements, the hardness of the HRC was obtained from the surface of the Fe-B based hard surface alloy layer was determined as 42.3 ± 1.7. The surface hardness values of Fe-Ti-B based hard surface alloy layers were changed between 46,3±4,1-57,2±5,1 HRC. The highest hardness value for this group of materials was observed in the composition of $Fe_8Ti_5B_7$. When the macro hardness curves seen in the figure are examined, it is observed that the hardness values of the alloy layer increase with the increase of the Ti element. Durmuş et al. stated in their study that the hardness of hard surface coatings depends largely on the fraction of primary hard phases and microstructure [23]. Gou et al. found that the hardness of the primary carbides was much higher than that of the eutectic matrix, and found that the increase in the volume fraction of primary carbides / borides increased the hardness of hard surface alloys [24]. There is a similar situation for the Fe-Ti-B based hard

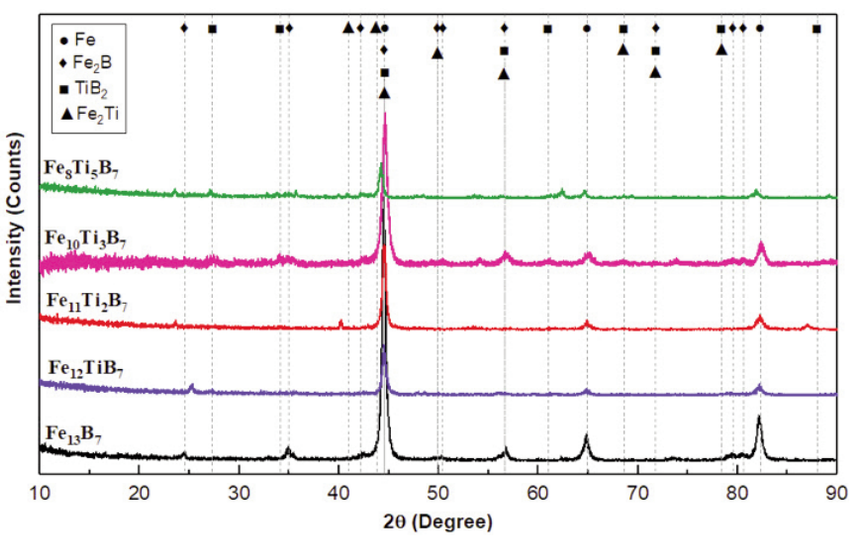

Figure 5. *X-ray diffraction pattern of $Fe_{(13-x)}Ti_xB_7$ (x= 0, 1, 2, 3 and 5) based hard surface alloyed steels*

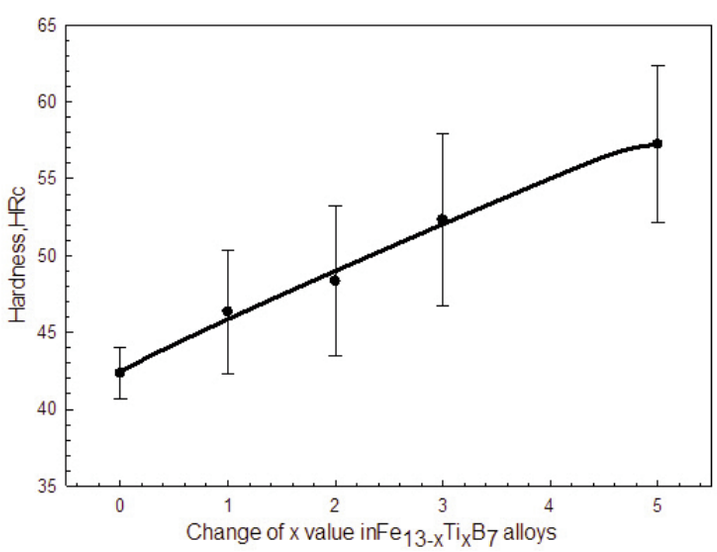

Figure 6. *Macro hardness of $Fe_{(13-x)}Ti_xB_7$ (x= 0, 1, 2, 3 and 5) based hard surface alloyed steels*

surface alloy system. It is seen that with the increase of the Ti ratio in the system, the amount of hard TiB_2 phase increases and the surface hardness increases in accordance with the above explanations.

In Figure 7 (a), the microhardness results of the produced coatings from the substrate to the surface are given at 0.1 mm intervals. The microhardness of hardfacing coatings is highly dependent on the volume fraction of the hard phases such as carbides and borides in the microstructure [21, 25, 26]. In general, it is seen from the graph that the microhardness increases with increasing Ti amount. This result can be explained by the presence of TiB_2 and eutectic phases, which have much higher hardness than α-Fe. It is also seen that there are partial fluctuations in the microhardness results. The reason for these fluctuations is due to the small hard phases such as TiB_2 in the microstructure [27]. On the other hand, according to the graph, it is seen that the microhardness values increase from the substrate to the coating layer. This is an indication that the coatings are carried out with the appropriate welding current value and the dilution is low.

Figure 7 (b) shows the phase hardness values obtained from the microhardness measurements of Fe-B, and Fe-Ti-B based hard surface alloys. As a result of the measurements, the hardness value of the substrate (SAE 1320 steel) was determined as 185 ± 9 $HV_{0.01}$. The hardness values of iron boride phases in Fe-B based hard surface alloys are 1901 ± 127 $HV_{0.01}$, the hardness of the eutectic structure (α-Fe+Fe_2B) is 897 ± 82 $HV_{0.01,}$ and the transition zone hardness is 369 ± 76 $HV_{0.01}$ as

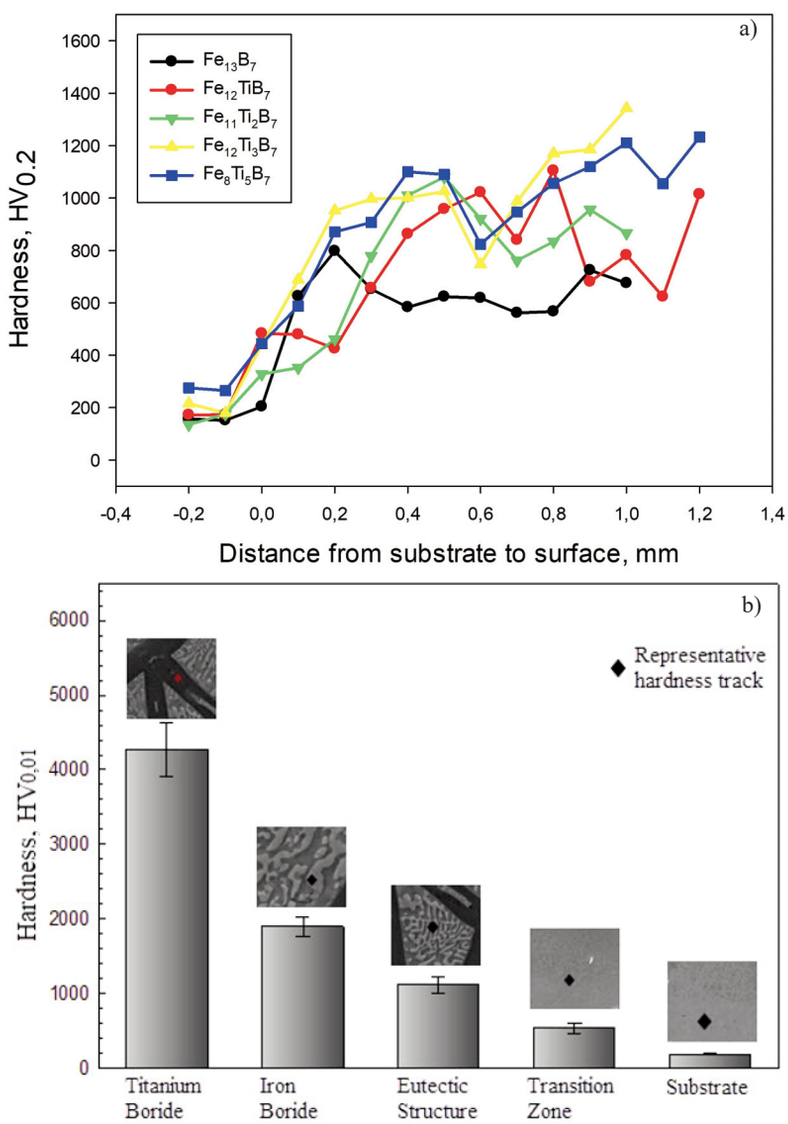

Figure 7. *(a) Microhardness distribution from substrate to surface (b) phase hardness of $Fe_{(13-x)}Ti_XB_7$ (x= 0, 1, 2, 3 and 5) based hard surface alloyed steels*

determined. The hardness of Fe_2B phase varies between 1100-2000 HV values [14, 20]. The measured hardness values are consistent with the data in the literature.

The hardness values of the titanium boride phases in the Fe-Ti-B based hard surface alloyed surface layer formed on the steel surface by GTA welding vary between 3804±291-4272±241 $HV_{0.01.}$ The highest hardness value for this phase was observed in $Fe_{11}Ti_2B_7$ and $Fe_8Ti_5B_7$ compositions. As a result of the literature reviews, the hardness values of the titanium boride phases vary between 2300-3930 HV [10, 14, 28]. It was observed that the hardness values measured were consistent with these studies. As a result of the measurements, there was no significant change in the hardness values with the increase in Ti ratio. The hardness values of the eutectic structure in the hard surface alloy layer changes between 1054±92-1148±43 $HV_{0.01}$. The hardness values of the transition zone in hard surface alloys vary between 484±12-537±76 $HV_{0.01}$.

3.3. Wear Behavior

The change of wear rates of Fe-B and Fe-Ti-B based hard surface alloy layers depending on the applied load is given in Figure 8. When the wear rate graph is examined; as stated in Archard equation [29], the increase in the load resulted in an increase in the rate of wear. In addition, it is seen that as the amount of Ti added increases, wear rates decrease for all applied loads. As a reason, it is thought that there is an increase in the amount of hard metal (Ti and Fe) boride phase in the hard surface alloy layer. Buytoz and Eren stated in their study that the increase in the amount of reinforcement in composite materials decreased the wear rate values [30]. As stated in the microstructure explanations, it is seen that the amount of high hardness TiB_2 phase increases due to the increase in the Ti ratio in the coating layer. The values obtained as a result of the hardness test clearly show that the macro hardness values of the samples increase with the increase of the Ti ratio. In accordance with these explanations, the wear performance of the coating layers increased with the increase of the Ti ratio. Among the coating layers, the lowest wear rate values were determined in the composition of $Fe_8Ti_5B_7$ for 2.5N, 5N and 10N loads.

While a 100% increase in load (from 2.5N to 5N) causes an increase in wear rate of 73.8% for Fe-B based hard surface alloy; When the increase in load is 300%, the increase in wear rate is 303.4%. This value caused an increase in the wear rate for ($Fe_{(13-x)}Ti_xB_7$) x = 1. 2. 3 and 5 at the rates of 142.7-501.8%, 123.1-445.4%, 125.6-403.9% and 142.6-419.6% respectively, depending on the increase in Ti ratio. Increases in value generally take place close to each other. As can be seen from the graphic, the increase in the amount of Ti has significantly decreased down to 69.6 %.

The SEM microstructure of the worn surfaces of Fe-B and Fe-Ti-B based hard surface alloys, which are subjected to wear tests under 0.1 m/s and 5N load, is shown in Figure 9. On the worn surface of the $Fe_{13}B_7$ composition given in Figure 9 (a-b), a small amount of abrasive wear mechanism was observed together with the adhesive wear. In addition, it is seen that the hard regions remain intact as the peak and the soft phases are eroded. In the Fe-Ti-B based hard surface alloy system given in Figure 9 (c-h), the main wear mechanism is adhesive, but there is also abrasive

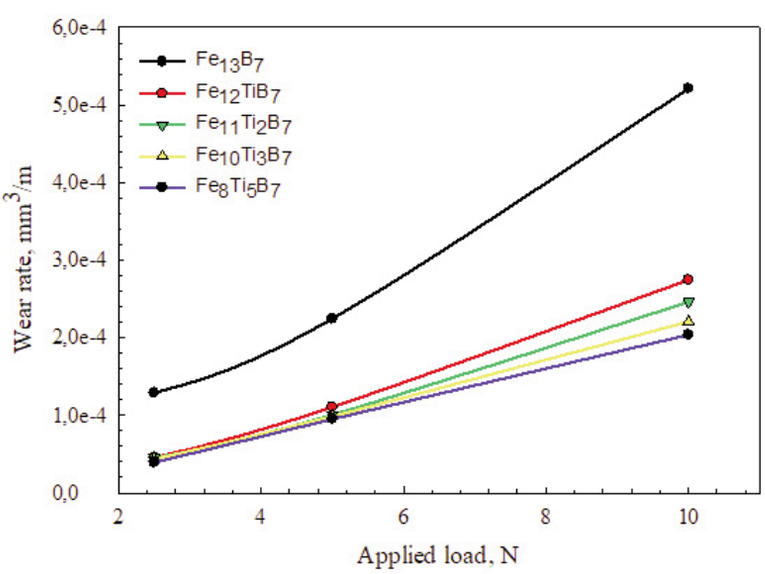

Figure 8. *Change of wear rates of Fe-B and $Fe_{(13-x)}Ti_XB_7$ (x= 0, 1, 2, 3 and 5) based hard surface alloy layers depending on load*

wear. Particularly, it is seen that the areas where the hard TiB_2 phase is present remain intact and the soft phases are eroded. Also, delamination wear was observed on the worn surfaces. SEM images showed that the worn debris oxidized due to friction, accumulated in hollow areas and plastered on the alloy layer. Therefore, it was observed that the worn surfaces of all samples were oxygen in EDS analysis (Figure 10). It was possible to say that the main wear mechanism had an adhesive and oxidative character. However, abrasive, delamination, and polishing wear were also detected on worn surfaces.

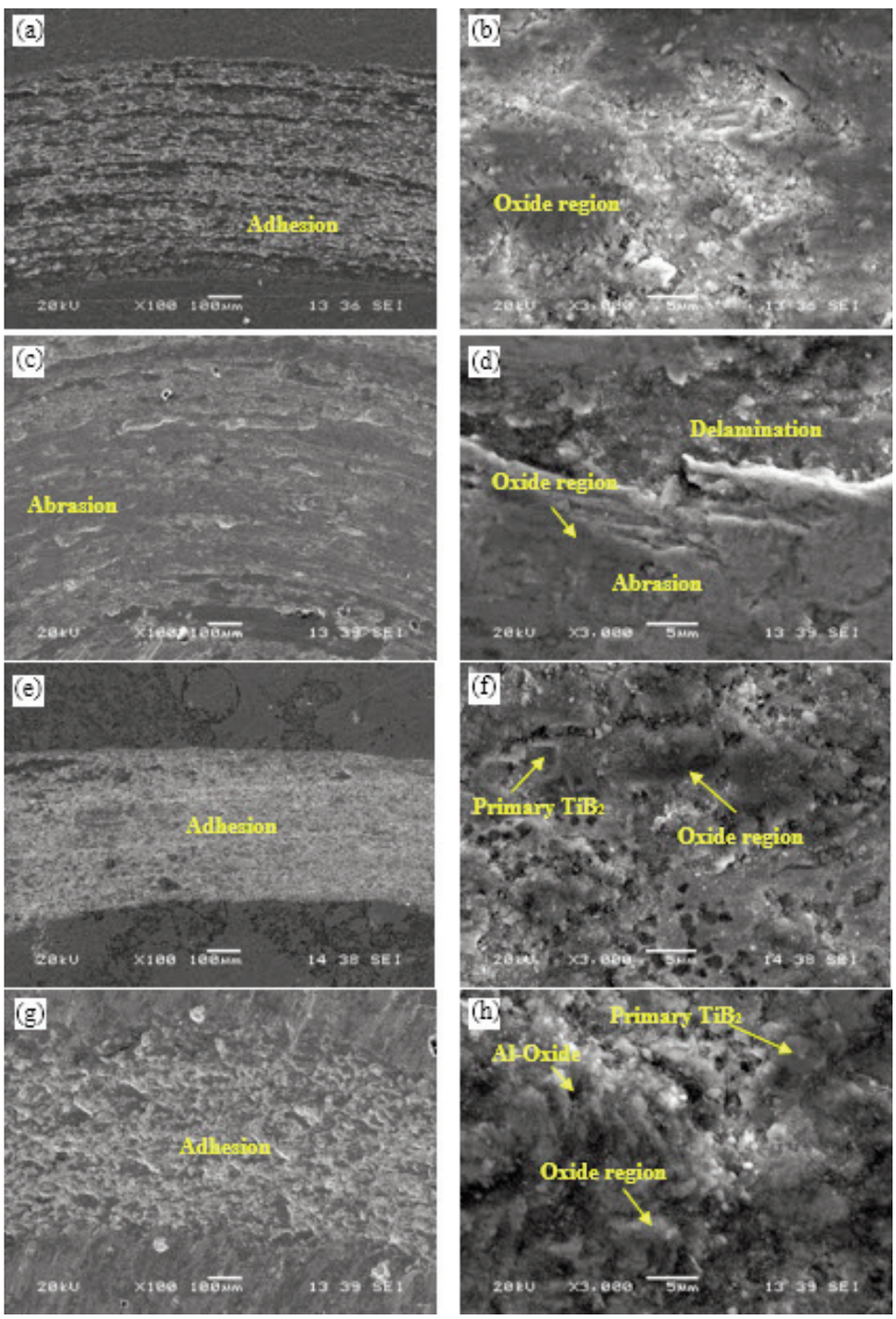

Figure 9. *The SEM micrographs of worn surfaces of samples tested at 5 N load: (a-b) $Fe_{13}B_7$ (c-d) $Fe_{12}Ti_2B_7$ (e-f) $Fe_{10}Ti_3B_7$ (g-h) $Fe_8Ti_3B_7$*

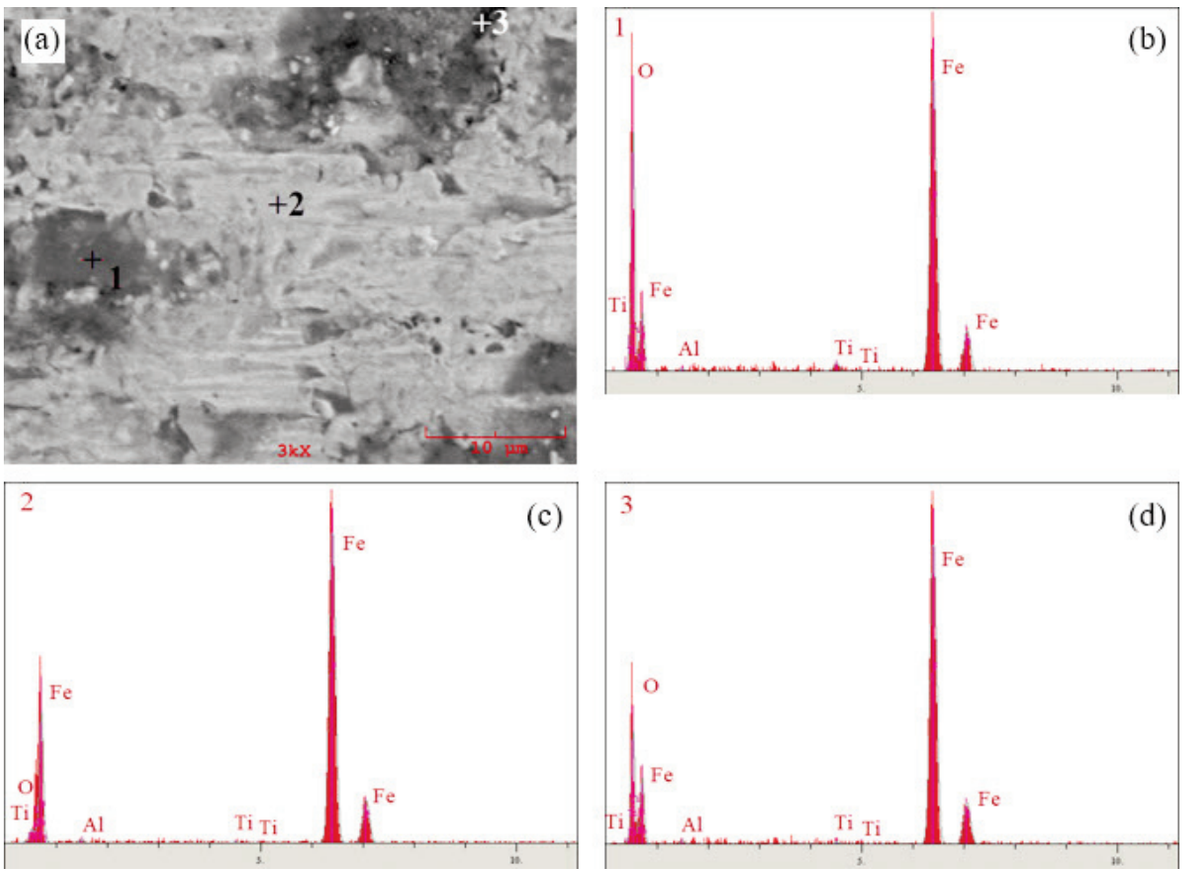

Figure 10. *(a) SEM microstructure image and (b-d) EDS analysis of $Fe_{12}TiB_7$ hard surface alloy worn surface under 5N load*

4. Conclusions

In this study, the effect of Ti element on microstructure and wear resistance in $Fe_{(13-x)}Ti_xB_7$ (x= 0, 1, 2, 3 and 5) based hard surface alloy layers was investigated. In line with the researches and experiments, the following results were reached:

1. The thickness of the coating layers produced by the TIG welding method was approximately 2-3 mm, and showed good bonding with the backing. It also has a non-porosity and smooth surface topography.

2. The Fe-B based alloy ($Fe_{13}B_7$) was composed of a hypereutectic primary Fe_2B massive phase and eutectic (α-Fe+Fe_2B) phases. In Fe-Ti-B alloys, as the amount of Ti increases, the TiB_2 phase density formed in the system increased and the TiB_2 phase transformed from an equiaxed structure to a rod-like and long sharp-edged structures. In addition, when titanium reached very high rates, the Fe_2Ti phase was formed in the eutectic structure.

3. X-ray diffraction analysis showed that the system included α-Fe, Fe_2B, TiB_2, and Fe_2Ti phases.

4. With the increase of titanium in the alloy composition, both macro and micro hardness values increased. The TiB_2 phase had a significant effect on the increase in the hardness of the coatings.

5. It was seen that as the amount of Ti added to the hard surface alloy layers increased, the wear rates decreased for all the applied loads. Among these alloys, it was determined that the best wear resistance belonged to the $Fe_8Ti_5B_7$ sample. In addition, the wear rate values of $Fe_{(13-x)}Ti_xB_7$ (x= 0, 1, 2, 3 and 5) alloy layers were lower than the wear rate values of $Fe_{13}B_7$ hard surface alloy layer.

6. The wear test results were directly related to the hardness of the hard surface alloys. Scanning electron microscope images of the worn surfaces showed that the main wear mechanisms were adhesive and oxidative. However, abrasive, delamination, and polishing wear were also seen on worn surfaces.

Acknowledgements

Authors are grateful to the financial support provided by Sakarya University Scientific Research Projects Unit with Project No. 2014-50-02-013.

Author's contributions

Dr. Bülent KILINÇ was responsible experimental designing, experimental studies and writing, Dr. Engin KOCAMAN was responsible writing and language. Prof. Dr. Şaduman ŞEN and Prof. Dr. Uğur ŞEN contributed the paper as senior authors.

Data availability

The datasets used or analyzed during the current study are available from the corresponding author on reasonable request.

Conflicts of interest

The authors declare that they have no known competing financial interests or personal relationships that could have appeared to influence the work reported in this paper.

References

[1] L. D. Olson, T. A. Siewert, S. Liu, G. R. Edwards, in ASM Handbook: Welding Brazing and Soldering, 8th ed. (E. H. Kottcamp), ASM International, America, 1993, p.1967

[2] M.F. Buchely, J.C. Gutierrez, L.M. Leon, A. Toro, The effect of microstructure on abrasive wear of hardfacing alloys, Wear, 259 (2005) 52–61. https://doi.org/10.1016/j.wear.2005.03.002

[3] E. Abakay, B. Kilinc, S. Sen, U. Sen, Wear properties of TIG surface alloyed steel with 50%Fe-10%W-40%B alloy, Acta Physica Polonica A, 127 (2015) 957–960. https://doi.org/10.12693/APhysPolA.127.957.

[4] K.Y. Chiu, F.T. Cheng, H.C. Man, Cavitation erosion resistance of AISI 316L stainless steel laser surface-modified with NiTi, Materials Science and Engineering: A, 392 (2005) 348–358. https://doi.org/10.1016/j.msea.2004.09.035.

[5] X.H. Wang, S.L. Song, S.Y. Qu, Z.D. Zou, Characterization of in situ synthesized TiC particle reinforced Fe-based composite coatings produced by multi-pass overlapping GTAW melting process, Surface and Coatings Technology, 201 (2007) 5899–5905. https://doi.org/10.1016/j.surfcoat.2006.10.042.

[6] Y.C. Lin, Y.H. Cho, Elucidating the microstructural and tribological characteristics of NiCrAlCoCu and NiCrAlCoMo multicomponent alloy clad layers synthesized in situ, Surface and Coatings Technology, 203 (2009) 1694–1701. https://doi.org/10.1016/j.surfcoat.2009.01.004.

[7] J.H. Chen, P.N. Chen, C.M. Lin, C.M. Chang, Y.Y. Chang, W. Wu, Characterization of multi-element alloy claddings manufactured by the tungsten inert gas process, Surface and Coatings Technology, 203 (2009) 2983–2988. https://doi.org/10.1016/j.surfcoat.2009.02.138.

[8] F. Madadi, M. Shamanian, F. Ashrafizadeh, Effect of pulse current on microstructure and wear resistance of Stellite6/tungsten carbide claddings produced by tungsten inert gas process, Surface and Coatings Technology, 205 (2011) 4320–4328. https://doi.org/10.1016/j.surfcoat.2011.03.076.

[9] B. Kilinc, O. Cegil, E. Abakay, U. Sen, S. Sen, Characterization of Fe-Nb-B base hardfacing of steel, Acta Physica. Polonica A, 125 (2014) 656–658. https://doi.org/10.12693/APhysPolA.125.656.

[10] L. Sun, Y. Gao, B. Xiao, Y. Li, G. Wang, Anisotropic elastic and thermal properties of titanium borides by first-principles calculations, Journal of Alloys and Compounds, 579 (2013) 457–467. https://doi.org/10.1016/j.jallcom.2013.06.119.

[11] Z.T. Wang, X.H. Zhou, G.G. Zhao, Microstructure and formation mechanism of in-situ TiC-TiB2/Fe composite coating, Transactions of Nonferrous Metals Society of China, 18 (2008) 831–835. https://doi.org/10.1016/S1003-6326(08)60144-2.

[12] M.R. Roshan, R. Taherzadeh Mousavian, H. Ebrahimkhani, A. Mosleh, Fabrication of Al-Based Composites Reinforced with Al2O3-TiB2 Ceramic Composite Particulates Using Vortex-Casting Method, Journal of Mining and Metallurgy, Section B: Metallurgy, 49 (2013) 299–305. https://doi.org/10.2298/JMMB120701032R.

[13] B. Stalin, M. Ravichandran, V. Mohanavel, L.P. Raj, Investigations Into Microstructure and mechanical properties of Mg-5wt.%Cu-TiB2 composites produced via powder metallurgy route, Journal of Mining and Metallurgy, Section B: Metallurgy, 56 (2020) 99–108. https://doi.org/10.2298/JMMB190315047S.

[14] S.O. Yilmaz, M. Ozenbas, TiB2-reinforced composite coating by gas tungsten arc welding, Journal of Materials Science, 44 (2009) 3273–3284. https://doi.org/10.1007/s10853-009-3443-6.

[15] M. Darabara, G.D. Papadimitriou, L. Bourithis, Production of Fe-B-TiB2 metal matrix composites on steel surface, Surface and Coatings Technology, 201 (2006) 3518–3523. https://doi.org/10.1016/j.surfcoat.2006.08.105.

[16] V. Raghavan, Phase Diagrams of Ternary Iron Alloys, Indian Institute of Metals, 1992, p.433.

[17] M. Ulutan, M. Yildirim, S. Buytoz, Investigation of microstructure of hardfaced AISI 4140 steel by TIG welding process, Journal of Engineering and Architecture Faculty of Eskişehir Osmangazi University, 12 (2009) 93–107.

[18] W. Shackelford, J. F., Alexander, Materials Science and Engineering, 3rd ed., CRC Press LLC, Washington, D.C., 2001, p.553.

[19] F. Zhou, C.M. Suh, S.S. Kim, R.I. Murakami, Sliding-wear behavior of TIN- and CrN-coated 2024 aluminum alloy against an Al2O3 ball, Tribology Letters, 13 (2002) 173–178. https://doi.org/10.1023/A:1020103908345.

[20] M. Eroglu, Boride coatings on steel using shielded metal arc welding electrode: Microstructure and hardness, Surface and Coatings Technology, 203 (2009) 2229–2235. https://doi.org/10.1016/j.surfcoat.2009.02.010.

[21] M.H. Amushahi, F. Ashrafizadeh, M. Shamanian, Characterization of boride-rich hardfacing on carbon steel by arc spray and GMAW processes, Surface and Coatings Technology, 204 (2010) 2723–2728. https://doi.org/10.1016/j.surfcoat.2010.02.028.

[22] A. Antoni-Zdziobek, M. Gospodinova, F. Bonnet, F. Hodaj, Solidification paths in the iron-rich part of the Fe-Ti-B ternary system, Journal of Alloys and Compounds, 657 (2016) 302–312. https://doi.org/10.1016/j.jallcom.2015.10.104.

[23] H. Durmuş, N. Çömez, C. Gül, M. Yurddaşkal, M. Yurddaşkal, Wear performance of Fe-Cr-C-B hardfacing coatings: Dry sand/rubber wheel test and ball-on-disc test, International Journal of Refractory Metals and Hard Materials, 77 (2018) 37–43. https://doi.org/10.1016/j.ijrmhm.2018.07.006..

[24] J. Gou, P. Lu, Y. Wang, S. Liu, Z. Zou, Effect of nano-additives on microstructure, mechanical properties and wear behaviour of Fe-Cr-B hardfacing alloy, Applied Surface Science, 360 (2016) 849–857. https://doi.org/10.1016/j.apsusc.2015.11.076.

[25] E. Kocaman, B. Kılınç, M. Durmaz, Ş. Şen, U. Şen, The influence of chromium content on wear and corrosion behavior of surface alloyed steel with Fe(16-x) Crx(B,C)4 electrode, Engineering Science and Technology, an International Journal, 24 (2021) 533–542. https://doi.org/10.1016/j.jestch.2020.08.003.

[26] B. Venkatesh, K. Sriker, V.S.V. Prabhakar, Wear Characteristics of hardfacing alloys: State-of-the-art, Procedia Materials Science, 10 (2015) 527–532. https://doi.org/10.1016/j.mspro.2015.06.002.

[27] E. Kocaman, B. Kılınç, Ş. Şen, U. Şen, Effect of chromium content on Fe(18-x) CrxB2(X=3,4,5) hardfacing electrode on microstructure, abrasion and corrosion behavior, Journal of the Faculty of Engineering and Architecture of Gazi University, 36 (2020) 177–190. https://doi.org/10.17341/gazimmfd.689230.

[28] S.O. Yilmaz, M. Ozenbas, M. Yaz, Synthesis of TiB2-reinforced iron-based composite coating, Tribology International, 42 (2009) 1220–1229. https://doi.org/10.1016/j.triboint.2009.04.041.

[29] V.K. Rai, R. Srivastava, S.K. Nath, S. Ray, Wear in cast titanium carbide reinforced ferrous composites under dry sliding, Wear, 231 (1999) 265–271.

[30] S. Buytoz, H. Eren, Effect of particle reinforcements on abrasive wear performance of aluminum metal matrix composites, Science and engineering Journal of Fırat University, 19 (2007) 209–216.

UTICAJ SADRŽAJA TITANIJUMA NA MIKROSTRUKTURU I PONAŠANJE PRI HABANJU $Fe_{(13-x)}Ti_xB_7$ (x=0-5) LEGURE ZA TVRDO NAVARIVANJE

B. Kılınç [a,*], E. Kocaman [b], Ş. Şen [c], U. Şen [c]

[a] Sakarija univerzitet primenjenih nauka, program za mašine i metale, Škola strukovnih studija Arifije, Arifije, Sakarija, Turska

[b] Univerzitet Bulent Edževit u Zonguldaku, Fakultet za inženjerstvo, Odsek za metalurško inženjerstvo i inženjerstvo materijala, Inčivez, Zonguldak, Turska

[c] Sakarija univerzitet, Fakultet za inženjerstvo, Odsek za metalurško inženjerstvo i i inženjerstvo materijala, Esentepe kampus, Sakarija, Turska

Apstrakt

U ovoj studiji je ispitivan uticaj dodavanja titanijuma na mikrostrukturu, tvrdoću, i stopu habanja čvrstih površinskih slojeva legure na bazi $Fe_{(13-x)}Ti_xB_7$ (x = 0, 1, 2, 3 i 5) formiranih metodom zavarivanja elektrolučnom volframovom elektrodom (GTA). Nakon ispitivanja mikrostruktura i faze analize, utvrđeno je da se strukture prevlaka sastoje od α-Fe, αFe+Fe_2B eutektičke, α-Fe+Fe_2Ti eutektičke i tvrde TiB_2 faze. U tvrdom površinskom sloju legure, kako je količina titanijuma povećavana, tako se i gustina TiB_2 faze u sistemu povećala, i primećeno je da se iz ekviaksijalne strukture formiraju štapičaste faze i faze dugih oštrih ivica. Kao rezultat ispitivanja habanja izvršenih pri različitim opterećenjima, utvrđeno je da dodavanje titanijuma smanjuje stopu habanja u sloju prevlake. Uz to, slike ishabanih površina dobijene skenirajućim elektronskim mikroskopom (SEM) pokazale su da su mehanizmi habanja bili adhezivni i oksidativni.

Ključne reči: *Tvrdo navarivanje; Legiranje površine; Fe-Ti-B legura; Borid; Tvrdoća; Habanje*